Biophysical Journal Volume 99 December 2010 3555–3562

Squeezing and Detachment of Living Cells

Marie-Josée Colbert,[†] Françoise Brochard-Wyart,[‡] Cécile Fradin,[†] and Kari Dalnoki-Veress[†*]
[†]Department of Physics & Astronomy and the Brockhouse Institute for Materials Research, McMaster University, Hamilton, Ontario, Canada; and [‡]Laboratoire de Physico-Chimie des Surfaces et Interface, Institut Curie, Paris, France

ABSTRACT The interaction of living cells with their environment is linked to their adhesive and elastic properties. Even if the mechanics of simple lipid membranes is fairly well understood, the analysis of single cell experiments remains challenging in part because of the mechanosensory response of cells to their environment. To study the mechanical properties of living cells we have developed a tool that borrows from micropipette aspiration techniques, atomic force microscopy, and the classical Johnson-Kendall-Roberts test. We show results from a study of the adhesion properties of living cells, as well as the elastic response and relaxation. We present models that are applied throughout the different stages of an experiment, which indicate that the contribution of the different components of the cell are active at various stages of compression, retraction, and detachment. Finally, we present a model that attempts to elucidate the surprising logarithmic relaxation observed when the cell is subjected to a given deformation.

INTRODUCTION

Of paramount importance to the function of cells are the interactions with their surroundings which are strongly dependent on their mechanical properties. To elucidate these properties, a variety of techniques have been developed and applied to parts of a cell, or to the entire cell (for example, see reviews (1–3)). Because cells actively respond to their environment, there has been much interest in methodologies that are able to probe the mechanosensory and dynamic properties of cells (4–12). For instance, the adhesion force developed by focal contacts can be mapped out using elastic micropatterned substrates (4). Another approach to measure the adhesion is to apply local force on a ligand to induce the detachment, such as with magnetic beads (8,9). Microbeads have also been used to study the elastic response of the cell to local deformation and the cytoskeleton (5,13). Similarly, atomic force microscopy has been used to probe the active response of the cytoskeleton (10–12,14,15).

On a larger lengthscale, there have been experiments to probe the mechanical properties of the cell in its entirety. Atomic force microscopy has been used to test the resistance of the entire cell to compression (16), and a microplate apparatus was developed to explore other aspects of the mechanical response of a single cell such as creep and viscoelasticity (17,18). Finally, an extensive series of studies have utilized the micropipette aspiration experiments that were first introduced by the seminal work of Evans et al. (19), which give measurements of the adhesion energy, the membrane tension, and the elastic modulus, while observations could be made with optical microscopy. The micropipette aspiration technique has also been refined to enable measurement of molecular adhesion (20) and to study the dynamics of unbinding (21).

The experiments discussed here build on these studies and measure the mechanical properties on the lengthscale of an entire cell. We have previously developed a micropipette deflection (MD) apparatus (22): a single cell is held at the end of a micropipette bent in an L-shape so that the deflection of the pipette can be used as a very precise force transducer. Though various configurations and sample types are possible, here we present results on cells pushed against a flat surface, allowed to relax, and then pulled away until detachment occurs. During the entire experiment, the force applied on the cell as well as its geometry are carefully monitored. The use of the negative pressure in the micropipette is only to hold the cell whereas the deflection of the pipette allows a 0.5 s temporal resolution.

Because of the cell's complexity, the analysis and the interpretation of the experimental data for techniques studying the cell as a whole are challenging. Theories often focus on the forces acting on the membrane, simplifying the system to the case of a liquid-filled closed membrane (20,23–25). Other models take the elastic response of the cell into account by considering the cell as an elastic bead (21,26). In this article, we find that different models describe the response of the cell at the different stages of the experiment, i.e., during compression, relaxation, retraction, and the final detachment from the adhesive surface. Furthermore, depending on the regime, either the membrane tension or the elastic properties of the cell dominate. The compression and retraction phases of the experiment are carried out fast enough (~10 s) that the models fit the data well with constant elastic properties. To be clear, the mechanosensory response of the cells do not dominate the elastic properties for the rapid compression and retraction measurements. One would expect that on longer timescale experiments, time-dependent elastic properties would be required to account for the cell's mechanosensory response. To investigate the response of a cell to external stresses on longer timescales, we carried out relaxation measurements.

Submitted January 28, 2010, and accepted for publication October 6, 2010.
*Correspondence: dalnoki@mcmaster.ca
Editor: Douglas Nyle Robinson.

0006-3495/10/12/3555/8 $2.00
doi: 10.1016/j.bpj.2010.10.008

The relaxation process is well explained by a simple phenomenological model motivated by the ideas of active processes in the living cell.

MATERIALS AND METHODS

The cell mechanics measurements were carried out in the MD apparatus, which is capable of high-resolution force measurement as a function of time, i.e., the dynamics is accessible (for further details on the instrumentation, see (22,27,28)). HeLa cells were suspended in a chamber made of two glass coverslips separated by two spacers. The chamber containing the cells was fixed atop a phase contrast microscope (IX71; Olympus, Melville, NY), and images recorded with a charge-coupled device camera (Retiga 2000R, QImaging, Surrey, British Columbia, Canada). The substrate used was made of a silicon wafer cleaned with filtered methanol before being coated with a 60 nm layer of gold. Gold deposition was carried out in an argon atmosphere (0.3 mbar), at a voltage of 1 kV, and a current of 30 mA (sputter coater, S150B; Edwards, Wilmington, MA). Substrates were used without any further cleaning. The substrate was fixed on a steel arm attached to a motorized translation stage (LTA-HS, controlled by ESP3000; Newport Instruments, San Diego, CA) and placed in the cell chamber.

The micropipettes were pulled from glass capillary tubes (inner diameter = 0.8 mm, outer diameter = 1 mm) to a final diameter of ~10 μm and a taper length of 15 mm. The pipette was then cut open and bent into an L-shape with a hot wire so that the section normal to the substrate and along the direction of translation was ~1 mm long. The spring constant of the pipette was calibrated by measuring the deflection resulting from the weight of a water droplet. Distilled water was injected into the pipette until a droplet was formed at the end of the pipette. As more water was injected, the diameter (and hence, the volume and the weight) of the droplet was monitored as well as the displacement of the pipette.

Pipette displacements were measured using optical microscopy and cross-correlation analysis of the images, both for the calibration and in regular use. The displacement resolution is ~0.1 μm. Typical values of the spring constant measured were between 1 and 10 nN/μm. The calibrated pipette was connected to a pressure controller (a variable height water reservoir), fixed onto a micromanipulator (PCS 5000; Burleigh Instruments, Fishers, NY), and also placed into the cell chamber. Because reducing vibration is crucial to the success of the measurements, the entire experimental setup was placed on an active vibration isolation table (MOD-1; Halcyonics, Menlo Park, CA).

HeLa cells were cultured in α-MeM medium to which was added 10% of fetal bovine serum, 1% of antibiotic PS, and 0.1% of antifungal fungizon. Before the experiment, cells were detached using trypsin and resuspended in the sample chamber of the MD setup. In a typical experiment, a cell is randomly chosen, grabbed with the small negative pressure of the pipette and brought to a fixed position. The substrate approaches the cell at a slow speed (2 μm/s), makes contact, and then pushes on the cell. The surface is then held fixed for a given time (typically 3 min) before retracting at the same speed. As the substrate retracts, it pulls on the cell until the final detachment from the surface. During the experiment, a picture is taken every half-second, allowing monitoring of the displacement of the pipette, the substrate, and the change in shape of the cell during the entire experiment cycle.

EXPERIMENT

In Fig. 1 is shown a schematic of the experimental geometry, optical images, the strain of the cell, the contact radius, and the force applied by the pipette on the cell as a function of the time. In the first step (1: compression), the cell is being compressed by the substrate, which results in a displacement (defined as negative) of the pipette, and a deformation of the cell. In the second step (2: relaxation), the substrate is held at a fixed position, during which time the cell relaxes as it accommodates the imposed deformation (note the small decrease in the magnitude of the force during the relaxation stage). In the third step (3: retraction), the substrate is pulled away from the cell, which brings the pipette back to its original position (zero force). In the fourth step (4: unbinding), the substrate continues its path while the cell is being put under increasing tension by the pipette which is now applying a positive force as the area of the cell's contact patch decreases. Eventually, the cell abruptly detaches (5: detachment) from the surface and the pipette goes back to its original position. The pull-off force can be directly measured from this graph. We note that the same numbering scheme for the different stages is used throughout this article.

RESULTS AND DISCUSSION

The behavior of the cell is very different depending on whether the cell is being pushed onto, or pulled off of, the

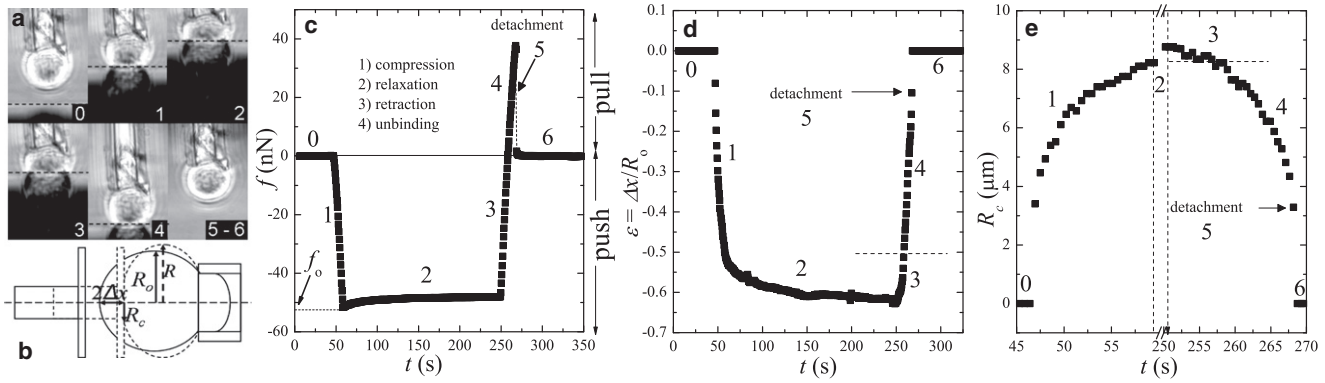

FIGURE 1 Typical experimental observations outlining the various stages of a cycle. The steps are numbered as follows: compression (stage 1); relaxation (stage 2); retraction (stage 3); unbinding (stage 4); and detachment (stage 5). In stages 0 and 6, there is no contact between the cell and substrate. (The substrate position is highlighted with a *dotted line*). Micrographs of the cell held by the pipette at various stages are shown in panel *a* with a corresponding sketch of the geometrical quantities monitored during the experiment (*b*). Note that in the micrographs the reflection of the cell in the substrate is visible, which facilitates finding the midplane. The force (*c*), strain (*d*), and contact radius (*e*) are shown as a function of time.

surface. We found that no single model could be used to analyze the entire response of the cell to the applied force in all stages. Rather, various models were needed to describe the data, which underlies the fact that at each stage different components of the cell dominate the behavior. Furthermore, the application of the various models provide different fundamental parameters (elastic properties, adhesion, or relaxation). We show in the Elastic Response section that when the cell is first being compressed into the substrate (stage 1), the stretching of the membrane dominates the elastic response and dictates the evolution of the contact radius. For this stage of the experiment, a liquid core-solid shell model was used to fit the elastic response (16). A second model (23), assuming an equilibrium of forces along the contour of the membrane, could be used to analyze the dynamics of the adhesion patch for the same experimental stage. Stage 2, the relaxation of the cell in response to the applied compression, can be understood at a phenomenological level and the model we have developed is discussed in the Logarithmic Relaxation section. The result of the relaxation process is that the cell's surface/volume ratio increases to accommodate the force applied by the pipette. Thus, after relaxation, excess surface has been created. The cell is retracted in stages 3 and 4, and is well adhered onto the surface. When the cell is pulled off the surface, the surface/volume ratio decreases and hence the membrane contribution is minimal. We assume that the entire cell is participating in the response as a viscoelastic body. Here we will simply take the cell to be an elastic body and ignore the viscous response because the pulling sequence lasts for only a few seconds.

Elastic response

The method presented allows a measurement of the strain of the cell, $\varepsilon = \Delta x/R_o$; here Δx is the deformation and R_o is the initial radius of the cell before compression. The strain provides a direct insight into the elastic response of the cell to the deformation when analyzed as a function of the applied force, f (see Fig. 2). In the first stage of the experiment (compression (stage 1), the substrate pushes on the cell and on the pipette with a force we define as negative, which compresses the cell. The force-extension curve follows a cubic behavior similar to a shell filled with an incompressible liquid that is stretching its membrane under a given load. In contrast with cases where strong adhesion has been established (12), pretension is negligible and the mathematical description is shown in detail by Lulevich et al. (29), with the final result,

$$f = 2\pi h R_o(\varepsilon - \varepsilon_o)^3\left(\frac{E_m}{1-\nu_m}\right), \quad (1)$$

where E_m is the Young's modulus of the membrane (including the cytoskeleton and assuming a homogeneous actin cortex), ν_m is the Poisson's ratio (1/2 for an incompressible membrane), h the thickness of the membrane, R_o the initial radius of the cell, ε the cell's strain, and ε_o the initial strain, which is set to zero for the first compression. This model does not take into account the deformation arising from the adhesion; thus, we apply it only to the first stages where the contact patch is negligible (see the Contact Region Behavior section for the discussion of the latter stages where the contact patch does plays a significant role).

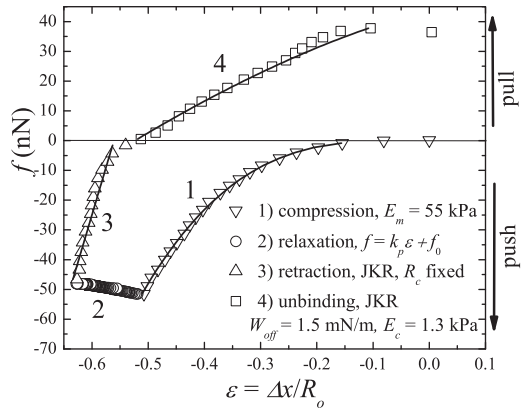

FIGURE 2 Force applied on the cell by the pipette as a function of the cell's strain. The experiment starts at zero force and zero strain. As the substrate pushes on the cell, the cell is being compressed and the pipette applies a negative force (stage 1). The experimental data points of the compression curve were fit (*solid line*) with Eq. 1. As the substrate is held fixed, the cell undergoes a relaxation process (stage 2). The substrate is then pulled away from the cell, starting the retraction stage of the experiment (stage 3). The experimental data points of the retraction curve were fit with Eq. 3 (*solid line*). As the substrate retracts, the cell remains attached to the surface and is put under tension by the pipette (stage 4), until it finally detaches. The experimental data points for the unbinding curve were fit with Eqs. 3 and 4 (*solid line*).

The agreement between the data and the model shown in Fig. 2 strongly suggests that the main response of the cell to the applied force is a stretching of the membrane. The value obtained for $E_m h$ is 5.5 ± 0.6 mN/m, resulting in an average Young's modulus of the membrane of $E_m = 55 \pm 6$ kPa when we assume an average membrane thickness of ~100 nm, which includes the actin cortex (30). The values obtained for $E_m h$ varies between 4 and 20 mN/m for a sample of 10 cells, which is comparable to similar studies done on T-cells with atomic force microcopy (16). Furthermore, the modulus of the membrane compares favorably with atomic force microscopy measurements, which probe local mechanical properties of the surface of HeLa cells (10,11).

In the second stage of the experiment, the substrate is held fixed, allowing the cell to relax under the imposed stress. During this time, the motion of the pipette is correlated with the deformation of the cell and therefore the force applied is

$$f = k_p\varepsilon + f_o, \quad (2)$$

where ε is the cell's strain, k_p is the spring constant of the pipette, and f_o is the force applied by the pipette when the substrate is stopped at the beginning of the relaxation. This equation represents the straight line observed in stage

2 of Fig. 2 and is discussed in further detail in Logarithmic Relaxation.

At the end of the relaxation process, the surface has expanded and the membrane is overstretched. As discussed in the Contact Region Behavior section, cellular adhesion is an active process that is time-dependent. Therefore, the relaxation process also allowed a strong adhesion to develop between the cell and the gold surface. The elastic characteristics of the cell are then dramatically changed by the presence of the excess surface and of the adhesion: the contribution of the membrane becomes minimal and the cell is acting as an elastic solid adhered onto a surface.

During the retraction stage of the experiment, the cell adopts two different regimes with a transition occurring when the cell is put under tension by the pipette (positive force). To analyze this regime, we use the classic Johnson-Kendall-Roberts (JKR) theory (31–33), which takes into account the presence of adhesion. The theory is based on the deformation of a Hertzian sphere and includes the contribution of the adhesion energy to take into account the nonzero contact radius when no load is applied. There are three different contributions to the total energy of the system: the energy necessary to deform the bead, the work done on the bead, and the adhesion energy. The JKR theory results in two main conclusions describing the compression and the radius of the contact patch (32,33): First, total compression of the cell can be written as the sum of two terms, one due to the deformation arising from the formation of the contact, δ_1, and a second one resulting from the elastic response of the cell to the load, δ_2. The total deformation of the cell is given by

$$\Delta x = \delta_1 + \delta_2 = \frac{R_c^2}{3R_o} + \frac{2f}{3R_cK}, \tag{3}$$

where the spring constant of the cell is

$$K = \frac{4}{3}\left(\frac{E_c}{1-\nu_c^2}\right),$$

with contact radius, R_c, equatorial radius, R, the initial radius of the cell, R_o, the Young's modulus of the cell, E_c, and the Poisson ratio for an incompressible bead, $\nu_c = ½$. Second, the contact radius can be written as

$$R_c^3 = \frac{R_o}{K}\left[f + 3\pi W R_o + \sqrt{6\pi W R_o f + (3\pi W R_o)^2}\right], \tag{4}$$

where W is the adhesion energy.

Fig. 1 *e* shows that the contact radius barely decreases during the first part of the retraction. As a result, the first term of Eq. 3 is constant and we obtain a linear relationship between the force and the strain. This linearity is observed in the retraction stage 3 of the experimental data presented in the Fig. 2.

Combining Eqs. 3 and 4, we can analyze the detachment stage 4 of the experiment. The agreement of the JKR model with the experimental data shown in Fig. 2 confirms that the cell is acting as an elastic rubber bead adhered onto a surface when the cell is retracted (stage 3) and in the last stage detached from the substrate (stage 4). The adhesion energy measured with this model is $W_{off} = 1.5$ mN/m and the Young modulus of the entire cell (assuming minimal contribution from the overstretched cytoskeleton) is $E_c = 1.3$ kPa, which is an order-of-magnitude lower than the calculated value for the cytoskeleton ($E_m = 55 \pm 6$ kPa).

For a sample of 10 cells, the average value is measured to be $\overline{E}_c = 1.7 \pm 0.4$ kPa. The fact that the modulus during retraction is so low (i.e., when the membrane is relaxed and the bulk of the cell dominates) confirms the cortical shell-liquid core model that states that the rigidity of the cell is dominated by the stretching of the membrane and the cytoskeleton.

An interesting picture of cell mechanics emerges from the application of the various models. We can summarize our results thus far as follows:

Stage 1: compression

Initially the membrane of the cell is unstretched and the surface/volume ratio is at a minimum. As the cell is deformed, the surface/volume ratio increases and the membrane stretching dominates the compression. There is little adhesion between the two surfaces as the cell comes into contact with the substrate. The cell can be modeled as a capsule filled with an incompressible viscous fluid, which is confirmed by the $f \sim \varepsilon^3$ curve in Fig. 2.

Stage 2: relaxation

The substrate motion is halted in the experiment. The cell relaxes to accommodate the deformation and its strain is directly linked to the motion of the pipette.

Stage 3: retraction

The substrate motion retracts. The membrane is fully stretched and the adhesion between the cell and the substrate is now significant, resulting in a contact patch. The decrease in contact radius during retraction is negligible because there is an excess of surface area as the surface/volume ratio decreases. The pipette pulls on the bulk of the cell because the membrane contribution is negligible and the cell can be modeled as a soft rubber bead with a constant contact patch (Eq. 3 with the first term constant).

Stage 4: unbinding

The cell is under tension, allowing the contact radius to decrease. The cell acts as an elastic rubber bead detaching from an adherent surface and follows the full JKR theory.

Contact region behavior

The dynamics of the contact patch is determined by the interplay of the adhesion and the tension in the membrane in the case of a core liquid-solid membrane body, or between the

adhesion and the elasticity of the cell in the case of an elastic body. As discussed in the previous section, how the cell is modeled is dependent on the stage:

1. During compression, the cell mechanics is dominated by the membrane resulting in a membrane with an incompressible fluid core model;
2. During retraction, the cell mechanics is dominated by the bulk of the cell resulting in an elastic body model.

To study the dynamics of adhesion energy and membrane tension during compression, we use a model that was developed by Brochard-Wyart and de Gennes (BWdG) (23). In this model, an equilibrium is assumed among the force applied by the pipette, the surface tension, and the bulk pressure. This condition is valid along the entire membrane which contains a liquid core. Solving the force balance equation at the apex of the cell and at the contact point,

$$\frac{f}{2\pi R} = \gamma\frac{\psi\sin\theta - \psi^2}{1-\psi^2}, \tag{5}$$

where $\psi = R_c/R$, γ is the membrane tension, and θ is the contact angle at the triple point. Note that this expression provides the membrane tension in terms of experimentally accessible quantities. The force balance of the interfacial tension at the triple point determines the contact angle, θ.

By combining the Young-Dupré equation,

$$W = \gamma[1-\cos(\theta)] \tag{6}$$

and Eq. 5, we obtain an expression of $f/2\pi R$ as a function of ψ with the only free parameters being the adhesion energy W and membrane tension γ,

$$\frac{f}{2\pi R} = \gamma\frac{\psi\sin[\arccos(1-W/\gamma)] - \psi^2}{1-\psi^2}. \tag{7}$$

In Fig. 3 we plot $f/2\pi R$ as a function of ψ with a best fit of Eq. 7 to the data for the compression stage 1. We find the data to be in excellent agreement with the BWdG model.

Contrary to simple vesicles (22), we observe hysteresis between the compression and retraction curve. Hysteresis can be observed in cases where adhesion is an active process that evolves in time such as a bead coated with polymer brushes (33). In this case, the hysteresis is attributed to the relaxation regime during which the cell's membrane actively rearranges itself to increase its adhesion to the surface. To explain the influence of this hysteresis on the adhesion, we introduce two different adhesion energies W_{on}, associated with the initial adhesion energy, and W_{off}, associated with a higher adhesion energy that has become possible after the rearrangement of the membrane during the relaxation phase of the experiment.

As expected, the adhesion energy in the first regime is very small, $W_{on} = 0.09 \pm 0.01$ mN/m, whereas the adhesion energy in the later stage on the experiment is more than an order of magnitude larger, $W_{off} = 1.5 \pm 0.1$ mN/m, confirming the dynamic nature of the cell attachment process to the surface. For a sample of 10 cells, it was noticed that the values for W_{on} are fairly constant, with an average of 0.2 ± 0.1 mN/m. The average value measured for W_{off} was 1.7 ± 0.7 mN/m. Because the value of the adhesion energy is much higher in the latter regime, the system needs an input of energy to undergo the transition between the on-regime and the off-regime. As a result, it is only when the cell is under tension that the system will have enough energy to decrease the contact radius and detach the cell.

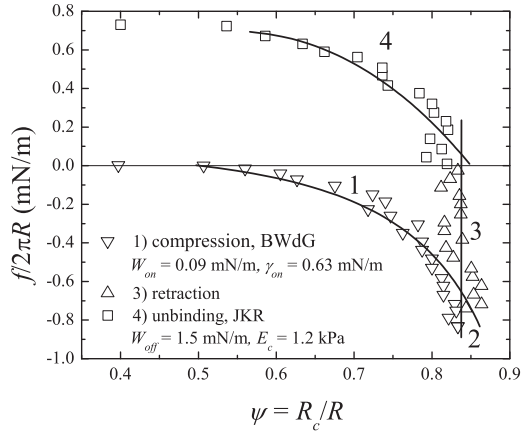

FIGURE 3 Force applied on the cell by the pipette as a function of the contact radius normalized by the equatorial radius. The experiment starts at zero force and zero contact radius. As the substrate pushes on the cell, the contact radius increases and the pipette applies a negative force (stage 1). The experimental data points were fit with Eq. 7 (*solid line*), from which the adhesion energy W_{on} and membrane tension are obtained. As the substrate retracts, the contact radius is first weakly affected by the change in the applied force (stage 3). As the substrate continues its retraction and puts the cell under tension, the contact radius starts decreasing with an increasing speed until the cell finally detaches from the substrate (stage 4). The experimental data points for the retraction curve was fit with Eq. 4 (*solid line*), from which the adhesion energy W_{off} can be obtained.

As mentioned previously, the contact radius can also be described in terms of the adhesion energy and the elastic constant of the cell in the JKR theory (Eq. 4). The quality of the fit for the unbinding part of the curve, which is presented in Fig. 3, supports again the dominance of the elastic response of the cell as a whole rather than the membrane during the unbinding of the cell. From this analysis, we find again a value for the adhesion energy is $W_{off} = 1.5$ mN/m and the Young's modulus of the cell is 1.2 mN/m, which is in excellent agreement with the values found in the last section (see Fig. 2). The various parameters obtained during the compression and retraction stages are summarized in Table 1.

Logarithmic relaxation

The last stage we discuss is also perhaps most intriguing. In the second stage of the experiment, the substrate is held fixed and the cell relaxes to accommodate the imposed deformation.

TABLE 1 Cell parameters obtained during the compression and decompression stages

Stage	Model	Parameters
Compression (1)	Lulevich	$E_m h = 5.5$ mN/m $E_m = 55$ kPa
	BWdG	$W_{on} = 0.09$ mN/m $\gamma_{on} = 1.2$ mN/m
Retraction stage (4)	JKR	$W_{off} = 1.5$ mN/m $E_c = 1.3$ kPa

Parameters and models described in the text. See also schematics in Fig. 5.

We stress here that this experiment is not a pure creep experiment, as the force varies slightly as the cell strain changes. However, because the force is constant to within 3% while there is a 20% change in the strain, analysis as a creep experiment is reasonable, an assumption that becomes even better at longer times. Surprisingly, the relaxation behavior shows a clear logarithmic dependence of the cell's strain over almost two orders of magnitude in time (see Fig. 4). This atypical time dependence of the relaxation suggests an activated process with metastable states separated by energy barriers (34–36). We present here a tentative model that is consistent with the data. Starting with the simple expectation that the rate of change of the strain is an activated relaxation process,

$$\frac{d\varepsilon}{dt} = -Ae^{-\Delta\omega/kT}, \tag{8}$$

where A is a constant, $\Delta\omega$ the energy barrier, and kT is the usual Boltzmann factor and temperature product. The relaxation is faster at the beginning of the process, which suggests an energy barrier that is smaller for smaller strain. On the contrary, as the total deformation of the cell has become large, the relaxation slows down, suggesting a higher energy barrier. We approximate the energy barrier as a Taylor expansion,

$$\Delta\omega/kT = a + b\varepsilon + c\varepsilon^2 + \dots, \tag{9}$$

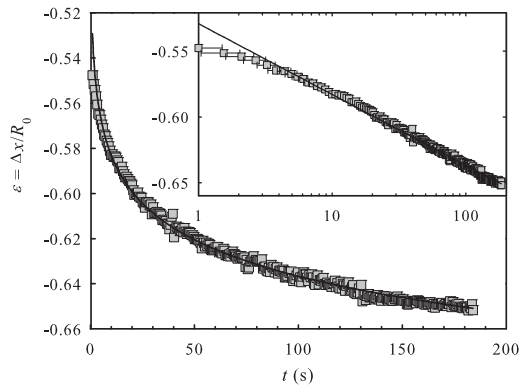

FIGURE 4 Strain of the cell as a function of time while the substrate is held fixed. This data is obtained from stage 2, during which the substrate is held fixed and the cell is relaxing. The semilogarithmic scale in the inset clearly shows the logarithmic time-dependence of the cell's relaxation. The lines are the best fit to Eq. 11.

with constants a, b, and c. Upon substitution of this energy barrier into Eq. 8, and keeping only the first order,

$$\frac{d\varepsilon}{dt} = -Ae^{-(a+b\varepsilon)}, \tag{10}$$

and the final result can be written as

$$\varepsilon = \frac{\ln(Abt)}{b} - \frac{a}{b} = \frac{\ln(t)}{b} - c. \tag{11}$$

In Fig. 4, the best fit to the Eq. 11 was obtained with $b = -4.29$ and $c = 0.528$. Relaxation experiments of the type shown in Fig. 4 were carried out with initial applied force ranging from 5 to 100 nN. In total, 120 relaxation experiments were carried out on 10 different cells. The constant c varies with experimental parameters like the initial compression. Because the prefactor to the logarithm is independent of the strain, ε, the model predicts that the rate of relaxation, parameterized by $1/b$ is a constant, independent of the initial compression. Remarkably, b remained constant to within 15% for all experiments. It is clear that this simplified phenomenological model does not take into account the biological complexity, and thus, cannot fully describe the relaxation process.

A further caveat is that, although the model presented captures the data over a broad range in time, it systematically fails to capture the early time response. Specifically, for the first few seconds of the relaxation experiment, the response is faster than that suggested by the logarithmic fit to the data (see Fig. 4). Neglecting the deviation from logarithmic time dependence of initial response, the data does support the idea of an activated process with a varying energy barrier between transitions, and only two parameters are required to describe the data. We find that a single power law cannot describe our data as well as the logarithmic relaxation, whereas a double power law as used by Pajerowski et al. (37) provides excellent agreement at the cost of requiring six fitting parameters. The relaxation of the type described by the model was robust and observed over a range of initial forces and for over 60 cells, including cells exposed to cytoskeletal drugs. The dependence of the relaxation on the addition of the cytoskeletal drugs nocodazole and cytochalasin D are the subject of a forthcoming publication.

CONCLUSIONS

The technique we developed provides accurate dynamic measurements of the adhesion of a single cell onto an adhesive substrate, as well as of the evolution of the elastic response of the cell to deformation. The response of the cell is complex and different under compression and retraction. In Fig. 5, we schematically summarize the different stages and the models used to analyze them.

During compression, stage 1, the adhesion energy is extremely low and the system is dominated by the stretching of the membrane. The analysis of the force-extension curve confirms that the cell's response is consistent with an

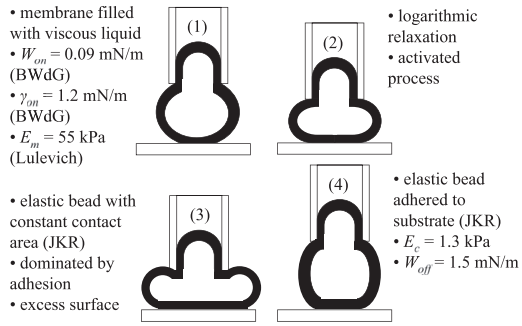

FIGURE 5 Summary of the experimental stages and of the analytical conclusions.

elastic membrane filled with an incompressible liquid: the membrane contributes most to the cellular mechanics during the initial compression. The relaxation stage 2 reveals a robust and surprising logarithmic time-dependence that holds more than two orders of magnitude in time and has been observed in ~60 living cells. We propose a simple, though purely phenomenological, model that correctly predicts the logarithmic relaxation. Only two parameters are required to fully describe the data. As predicted by the model, the relaxation rate is constant to within 15% over 120 relaxation experiments while the initial compression force is varied. The model is based on an activated process with an energy barrier that decreases with the strain. We note that logarithmic relaxation is seen in other strongly interacting complex systems such as granular materials, spin-glasses, and proteins (38).

During the retraction stages 3 and 4, it was found that after the cell has been in contact with the substrate for several minutes, the cell's membrane rearranges to maximize the adhesion, thus leading to a much higher adhesion energy. As the cell is being pulled off the surface, we observe that the mechanics of the cell is no longer dominated by the membrane, but is dictated by the elastic response of the whole cell. The transition from membrane-dominated during compression to bulk-dominated during retraction is found because, during the compression and relaxation stages, the surface/volume ratio increases (i.e., membrane must stretch, and then relaxes in this state) while the opposite is true for retraction. In stage 3, the cell retracts, but the contact patch does not decrease noticeably. When the force applied by the pipette passes a threshold, stage 4, the contact patch decreases until the cell eventually is released from the substrate. The final adhesion energy can be measured using the JKR theory for a soft rubber bead.

The simple nature of the experimental data offers the opportunity to measure important physical parameters such as the adhesion energy as the cell is brought into contact, $W_{on,}$ and pulled off the substrate, W_{off}, the membrane tension, γ, and the Young's modulus of the membrane, $E_{m,}$ and of the cell, $E_{c.}$ The successful application of the various models reveals which mechanical elements dominate as a stress is applied. However, there is also a very clear limitation of the models as they are applied to the compression and retraction phases of the experiment: the mechanosensory responses of the cell must result in elastic properties that vary as a function of time on longer timescales (4–9,39). Simply put, constant elastic properties successfully describe the data here only because the compression and retraction were carried out quickly compared to the mechanosensory responses of the cells. As shown by the relaxation stage, on long timescales the response of living cells is much more complex and cannot be described with constant elastic properties. Taken together, these results provide a more general understanding of the active response of the cell to its surroundings through the interplay between the adhesion and the elastic response to deformation. It is hoped that the experiments provide insight which will facilitate development of a single theoretical model that can describe the stress-strain relationship of living cells.

Financial support from the Natural Sciences and Engineering Research Council (Canada) and the American Chemical Society Petroleum Research Fund are gratefully acknowledged.

REFERENCES

1. Hochmuth, R. M. 2000. Micropipette aspiration of living cells. *J. Biomech.* 33:15–22.
2. Lim, C. T., E. H. Zhou, and S. T. Quek. 2006. Mechanical models for living cells—a review. *J. Biomech.* 39:195–216.
3. Hoffman, B. D., and J. C. Crocker. 2009. Cell mechanics: dissecting the physical responses of cells to force. *Annu. Rev. Biomed. Eng.* 11: 259–288.
4. Balaban, N. Q., U. S. Schwarz, …, B. Geiger. 2001. Force and focal adhesion assembly: a close relationship studied using elastic micropatterned substrates. *Nat. Cell Biol.* 3:466–472.
5. Bursac, P., G. Lenormand, …, J. J. Fredberg. 2005. Cytoskeletal remodeling and slow dynamics in the living cell. *Nat. Mater.* 4: 557–561.
6. Bershadsky, A., M. Kozlov, and B. Geiger. 2006. Adhesion-mediated mechanosensitivity: a time to experiment, and a time to theorize. *Curr. Opin. Cell Biol.* 18:472–481.
7. Ren, Y., J. C. Effler, …, D. N. Robinson. 2009. Mechanosensing through cooperative interactions between myosin II and the actin crosslinker cortexillin I. *Curr. Biol.* 19:1421–1428.
8. Guttenberg, Z., A. Bausch, …, E. Sackmann. 2000. Measuring ligand-receptor unbinding forces with magnetic beads: molecular leverage. *Langmuir.* 16:8984–8993.
9. Feneberg, W., M. Aepfelbacher, and E. Sackmann. 2004. Microviscoelasticity of the apical cell surface of human umbilical vein endothelial cells (HUVEC) within confluent monolayers. *Biophys. J.* 87: 1338–1350.
10. Gigler, A., M. Holzwarth, and O. Marti. 2007. Local nanomechanical properties of HeLa-cell surfaces. *In* Journal of Physics: Conference Series, Vol. 61. Institute of Physics Publishing, London, UK. p.780.
11. Leporatti, S., D. Vergara, …, R. Rinaldi. 2009. Cytomechanical and topological investigation of MCF-7 cells by scanning force microscopy. *Nanotechnology.* 20:055103.
12. Sen, S., S. Subramanian, and D. E. Discher. 2005. Indentation and adhesive probing of a cell membrane with AFM: theoretical model and experiments. *Biophys. J.* 89:3203–3213.
13. Trepat, X., L. Deng, …, J. J. Fredberg. 2007. Universal physical responses to stretch in the living cell. *Nature.* 447:592–595.

14. Lee, G., D. Kidwell, and R. Colton. 1994. Sensing discrete streptavidin-biotin interactions with atomic force microscopy. *Langmuir.* 10:354–357.

15. Wu, H. W., T. Kuhn, and V. T. Moy. 1998. Mechanical properties of L929 cells measured by atomic force microscopy: effects of anticytoskeletal drugs and membrane crosslinking. *Scanning.* 20:389–397.

16. Lulevich, V., T. Zink, …, G. Y. Liu. 2006. Cell mechanics using atomic force microscopy-based single-cell compression. *Langmuir.* 22: 8151–8155.

17. Desprat, N., A. Richert, …, A. Asnacios. 2005. Creep function of a single living cell. *Biophys. J.* 88:2224–2233.

18. Thoumine, O., and A. Ott. 1997. Time scale dependent viscoelastic and contractile regimes in fibroblasts probed by microplate manipulation. *J. Cell Sci.* 110:2109–2116.

19. Evans, E., D. Berk, and A. Leung. 1991. Detachment of agglutinin-bonded red blood cells. I. Forces to rupture molecular-point attachments. *Biophys. J.* 59:838–848.

20. Evans, E., K. Ritchie, and R. Merkel. 1995. Sensitive force technique to probe molecular adhesion and structural linkages at biological interfaces. *Biophys. J.* 68:2580–2587.

21. Pierrat, S., F. Brochard-Wyart, and P. Nassoy. 2004. Enforced detachment of red blood cells adhering to surfaces: statics and dynamics. *Biophys. J.* 87:2855–2869.

22. Colbert, M. J., A. N. Raegen, …, K. Dalnoki-Veress. 2009. Adhesion and membrane tension of single vesicles and living cells using a micropipette-based technique. *Eur. Phys. J. E Soft Matter.* 30:117–121.

23. Brochard-Wyart, F., and P. de Gennes. 2003. Unbinding of adhesive vesicles. *C. R. Phys.* 4:281–287.

24. Heinrich, V., and C. Ounkomol. 2007. Force versus axial deflection of pipette-aspirated closed membranes. *Biophys. J.* 93:363–372.

25. Simson, D. A., F. Ziemann, …, R. Merkel. 1998. Micropipet-based pico force transducer: in depth analysis and experimental verification. *Biophys. J.* 74:2080–2088.

26. Chu, Y. S., S. Dufour, …, F. Pincet. 2005. Johnson-Kendall-Roberts theory applied to living cells. *Phys. Rev. Lett.* 94:028102.

27. Nassoy, P. 2009. Commentary on "Adhesion and membrane tension of single vesicles and living cells using a micropipette-based technique" by M.-J. Colbert et al. *Eur. Phys. J. E Soft Matter.* 30:123–124.

28. Crosby, A. J. 2009. Commentary on "Adhesion and membrane tension of single vesicles and living cells using a micropipette-based technique" by M.-J. Colbert et al. *Eur. Phys. J. E Soft Matter.* 30:125–126.

29. Lulevich, V. V., D. Andrienko, and O. I. Vinogradova. 2004. Elasticity of polyelectrolyte multilayer microcapsules. *J. Chem. Phys.* 120: 3822–3826.

30. Cheng, Y., C. A. Hartemink, …, C. F. Dewey, Jr. 2000. Three-dimensional reconstruction of the actin cytoskeleton from stereo images. *J. Biomech.* 33:105–113.

31. Johnson, K., K. Kendall, and A. Roberts. 1971. Surface energy and the contact of elastic solids. *Proc. R. Soc. Lond. A Math. Phys. Sci.* 324:301–313.

32. Gérardin, H., A. Burdeau, …, F. Brochard-Wyart. 2007. Forced detachment of immersed elastic rubber beads. *Langmuir.* 23:9704–9712.

33. Gérardin, H. 2006. Crosslinked polymer: detachment-specific swelling [Polymère réticulés: détachement spécifique et gonflement]. PhD thesis. Université Pierre et Marie Curie, Paris, France.

34. Bell, G. I. 1978. Models for the specific adhesion of cells to cells. *Science.* 200:618–627.

35. Matan, K., R. B. Williams, …, S. R. Nagel. 2002. Crumpling a thin sheet. *Phys. Rev. Lett.* 88:076101.

36. Jaeger, H. M., Ch. Liu, and S. R. Nagel. 1989. Relaxation at the angle of repose. *Phys. Rev. Lett.* 62:40–43.

37. Pajerowski, J. D., K. N. Dahl, …, D. E. Discher. 2007. Physical plasticity of the nucleus in stem cell differentiation. *Proc. Natl. Acad. Sci. USA.* 104:15619–15624.

38. Brey, J. J., and A. Prados. 2001. Linear response of vibrated granular systems to sudden changes in the vibration intensity. *Phys. Rev. E Stat. Nonlin. Soft Matter Phys.* 63:061301.

39. Semmrich, C., T. Storz, …, K. Kroy. 2007. Glass transition and rheological redundancy in F-actin solutions. *Proc. Natl. Acad. Sci. USA.* 104:20199–20203.